Development of a High-Energy Electron Spectrometer For the Study of Lepton-Catalyzation in Nuclear Fusion Reactions

Tayler S Martin

A senior thesis submitted to the faculty of
Brigham Young University
in partial fulfillment of the requirements for the degree of

Bachelor of Science

John Ellsworth, Advisor

Department of Physics and Astronomy

Brigham Young University

ABSTRACT

Development of a High-Energy Electron Spectrometer For the Study of Lepton-Catalyzation in Nuclear Fusion Reactions

Tayler S Martin
Department of Physics and Astronomy, BYU
Bachelor of Science

Stellar fusion, the process powering stars, relies on overcoming the Coulomb barrier between charged particles, causing hydrogen's fusion into helium. Despite existing models, laboratory experiments show fusion rates that deviate by a factor of 2, suggesting a gap in our understanding. A promising theory proposes that leptons such as electrons could catalyze fusion inside the orbital radius. This concept, initially explored by S. Jones using muons at BYU, opens new avenues for experimentation. Our work extends this idea to electrons which could explain the discrepancy between theory and experiment regarding screening ability. We have developed an accelerator-target system, employing various metal targets and detectors, to investigate this phenomenon. A critical component of our experiment is a high-energy electron spectrometer, designed to detect and analyze electron products during fusion processes. This spectrometer has been calibrated against known beta-decay sources including cesium-137, europium-154, and strontium-90.

Keywords: Lepton-Catalyzed Fusion, High-Energy Electron Spectrometer

ACKNOWLEDGMENTS

I wish to express my deepest appreciation to my advisor, John Ellsworth. Working with him has been one of the greatest blessings of my undergraduate career, and he has become a dear friend. I also want to express my gratitude to my first advisor, Branton Campbell, who has perfected the art of mentoring. He gave me my first taste of research and helped me stretch beyond my limits.

I want to thank my family—my parents, Jeff and Mishele, and my siblings, Ryan, Amber, Jason, and Eric—for their continual support during this journey. They have kept me grounded by reminding me of the things that matter most in life.

Additionally, I am deeply grateful to the Brigham Young University College of Physical Mathematical Sciences and the Department of Physics and Astronomy for providing me with a research assistantship position and for providing the lab and equipment necessary to perform these experiments. I am particularly grateful for the College for funding the construction of the neutron detector. This opportunity has been invaluable in my pursuit of scientific research and academic growth.

I would also like to express my heartfelt gratitude to my grandfather, Ray Martin, who showed me the exciting and adventurous side of science and taught me that I could be both scientific and religious.

Finally, I want to express my appreciation and love for my God, for giving me a glimpse of His marvelous creations. His presence has been a guiding light throughout my studies.

Contents

Chapter 1

Introduction

At the heart of nuclear astrophysics is the study of fusion, a process where light nuclei combine to form heavier nuclei, releasing energy in the process. This phenomenon not only fuels stars but also plays a crucial role in the elemental makeup of the universe. Despite its significance, there's a persistent issue in fusion research: the predicted fusion rates in stars and what we've observed in the lab don't always align [1]. This discrepancy points to gaps in our understanding of fusion's fundamental principles, sparking curiosity and driving further investigation.

Muon-catalyzed fusion has been a focal point in exploring how we might overcome the repulsive forces between nuclei to facilitate fusion at lower energies. By introducing muons, which are like heavier versions of electrons, into the fusion environment, researchers have managed to get nuclei closer together (see Figure 1.1), producing over 150 reactions per muon [3]. However, the ability of using muons is limited because they're challenging to produce and have a finite lifetime of 2.2 microseconds. This brings us to an intriguing possibility: what if electrons, which are far more common and manageable, could be used to catalyze fusion in a similar manner?

This question led to the experimental efforts by Lipoglavsek and his team in 2017. They attempted to detect electron-induced fusion by observing reactions in a deuterium beam experiment, hoping to see evidence of electrons playing a significant role in fusion events [4]. However, their

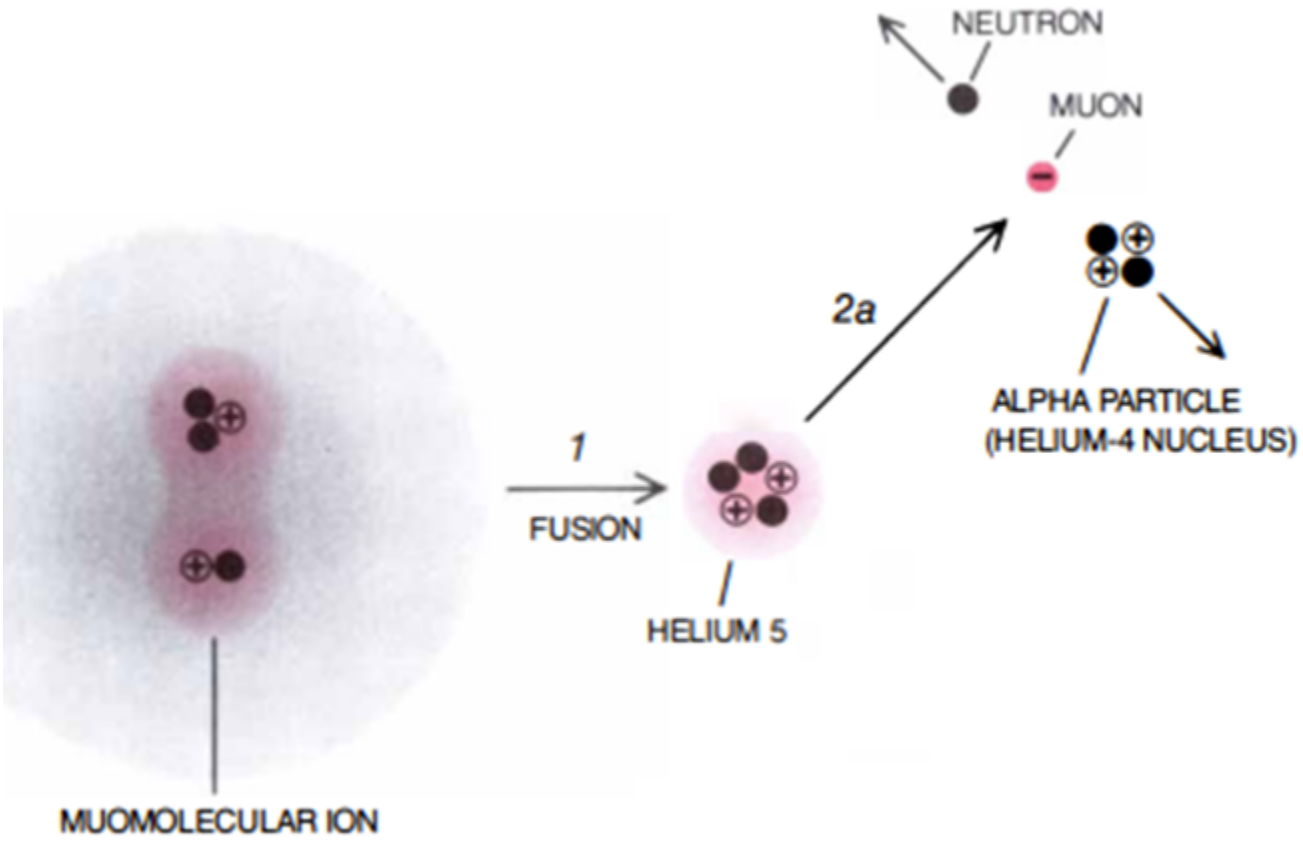

Figure 1.1 Simple drawing demonstrating how muons pull nuclei together to fuse. After fusion, the muon is re-emitted to catalyzed future reactions. [2]

experiment faced limitations, primarily due to the inability to lower the beam energy sufficiently to enhance the fusion cross-section, which is crucial for observing such events [5].

Our research aims to tackle this challenge head-on. With access to technology that allows us to reduce the beam energy to as low as 5 keV, we're in a unique position to explore the possibility of electron-catalyzed fusion more thoroughly. We're looking for electrons with energies indicative of enhancing fusion reaction rates by examining proton-deuterium (p+d) and deuterium-deuterium (d+d) reactions [6]. Our setup includes an accelerator-target system [4] [7] [8] and a high-energy electron spectrometer, specifically designed to detect the high-energy electrons indicative of fusion.

By investigating how electrons might impact fusion rates, we're also contributing to the broader discussion about why there's a difference between the fusion rates we calculate based on our electron-screening theories and those we observe in the lab [1]. If we can show that electrons, like muons, can catalyze fusion, we'll not only advance our knowledge of fusion but also take a step toward resolving a long-standing puzzle in nuclear astrophysics.

In this thesis, I describe the design of the high-energy electron spectrometer as well as the testing and calibration process to prepare it for the fusion experiments described previously.

Chapter 2

Experimental Setup

To initiate fusion reactions, we employ an energetic ion source that generates a beam of deuterium ions. These ions are directed towards a metal target infused with hydrogen or deuterium. The metal not only provides structural integrity but also contributes conduction electrons, which facilitate Coulomb screening, potentially enhancing the efficacy of the fusion reactions [8]. This target is centrally positioned within a target vacuum chamber, where the beam is introduced.

Surrounding the vacuum chamber are a suite of detectors strategically positioned to analyze the fusion reactions by capturing and characterizing the reaction products and their energies (see Figure 2.1). This suite includes an energy-dispersive X-ray spectrometer (see Appendix A), an ΔE-E charged-particle spectrometer (see Appendix B), a high-purity germanium gamma spectrometer, an LGB gated neutron pseudo-spectrometer [9], and a high-energy electron spectrometer. Each detector plays a vital role in identifying different aspects of the reaction outputs, ensuring confidence in our analysis of the fusion events.

Included with the suite of detectors is a Perkin Elmer Model 04-303 Differential Ion Gun [10]. This is used as a 0-5 keV ion source to stimulate the fusion reactions via inverse kinematics. There is also an electron gun and a 400 keV Van der Graaf particle accelerator for the purpose of doing elemental analysis of the target material.

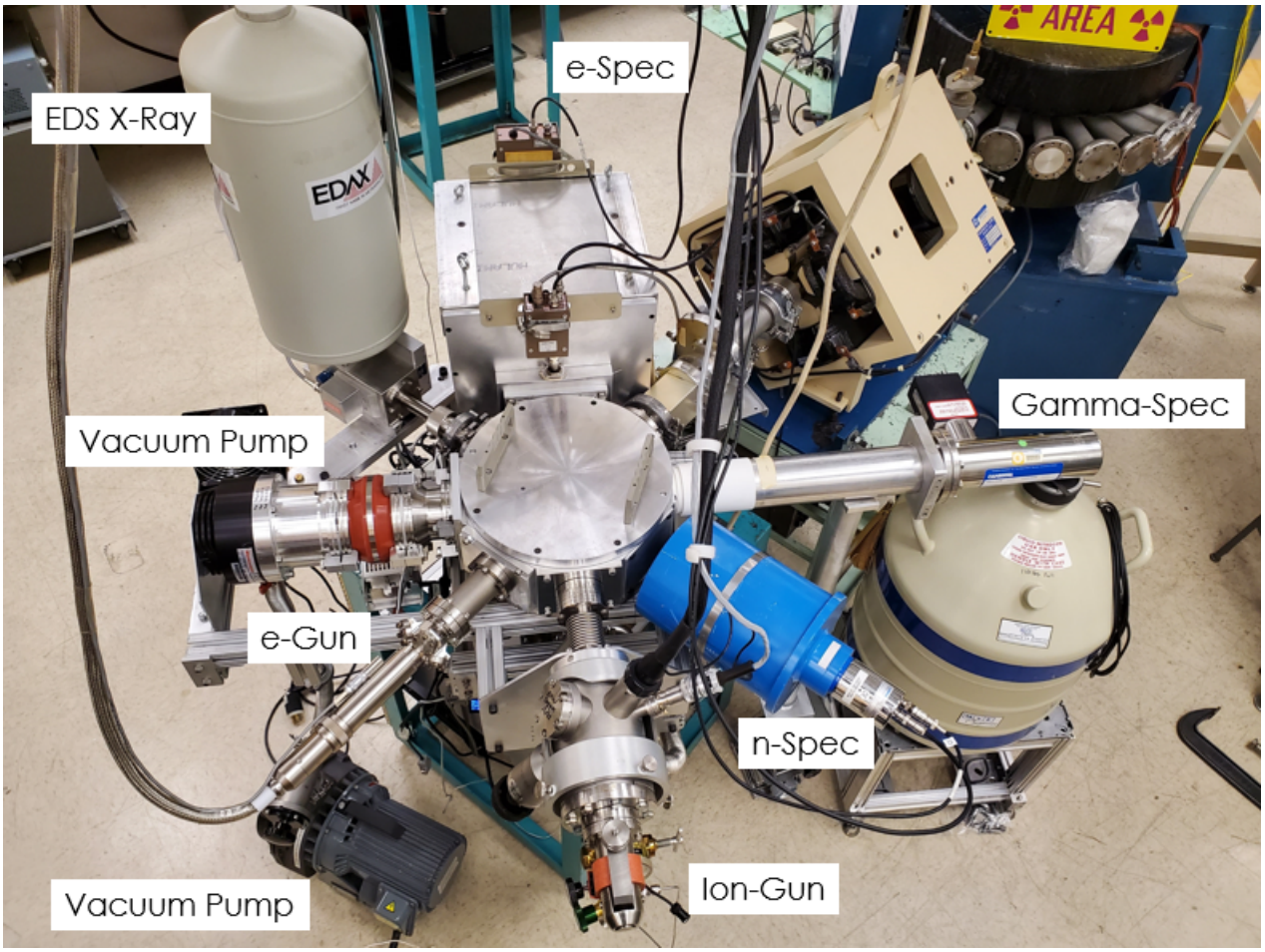

Figure 2.1 Bird's-eye view of the entire accelerator-target apparatus, highlighting the separate detectors used to identify the occurrence and pathways of reactions.

My contributions focused on configuring the vacuum chamber and designing the electronics that process signals from these detectors, particularly the high-energy electron spectrometer. The precision in configuring these elements is crucial for determining if electrons significantly catalyze fusion beyond the effects of Coulomb screening.

The electron spectrometer is an Elgin model EJ200 which is a 10 liter block of PVT scintillator 30.5 cm high, 30.5 cm wide and 15cm deep which was calculated to absorb the energy of electrons up to 25 MeV. Scintillations are viewed by four photomultiplier tubes (PMT) from which pulses are amplified and recorded by a Multichannel Analyzer (MCA), the amplitude or height of the resulting pulses being proportional to the energy of the detected electrons. PVT is also an efficient cosmic and background gamma ray detector. To discriminate for electrons against gamma rays a gamma insensitive thin silicon surface-barrier detector is installed ahead of the PVT. This detector covers an area of 2000 mm^2 and is 300 microns thick, absorbing energy at a rate of 0.4 keV per micron thickness [11]. It is reversed biased using an Ortec 428 set to 70 V. The amplified pulses are processed and applied to a linear gate that interrupts the PVT signal and allows only pulses from electrons to be recorded.

Figure 2.2 shows light from electron scintillations is collected by four photo-multiplier tubes(PMTs) [12] each supplied with a positive bias by an Ortec 556 high voltage power supply (not shown). Each of the 556 supplies are nominally set to 1200VDC and adjusted a few volts up or down as needed to make the gain of each PMT match each other. Their output pulses are ganged together with a 93 ohm combiner and fed to an Ortec 113 Scintillation Amplifier [13] set to 1 nF, which serves as a preamplifier. Pulses are then shaped and amplified using an Ortec 575A spectroscopy amplifier [14] set to receive negative inputs and a gain of 6.38. The output is then sent to an Ortec 590A SCA amplifier [15] set to a gain of 2.5 and produces a positive, unipolar output.

The thin silicon detector discriminates for electrons by providing a signal of its own. However, this must be timed coincidentally with the proper PVT signal. The signal from the silicon detector

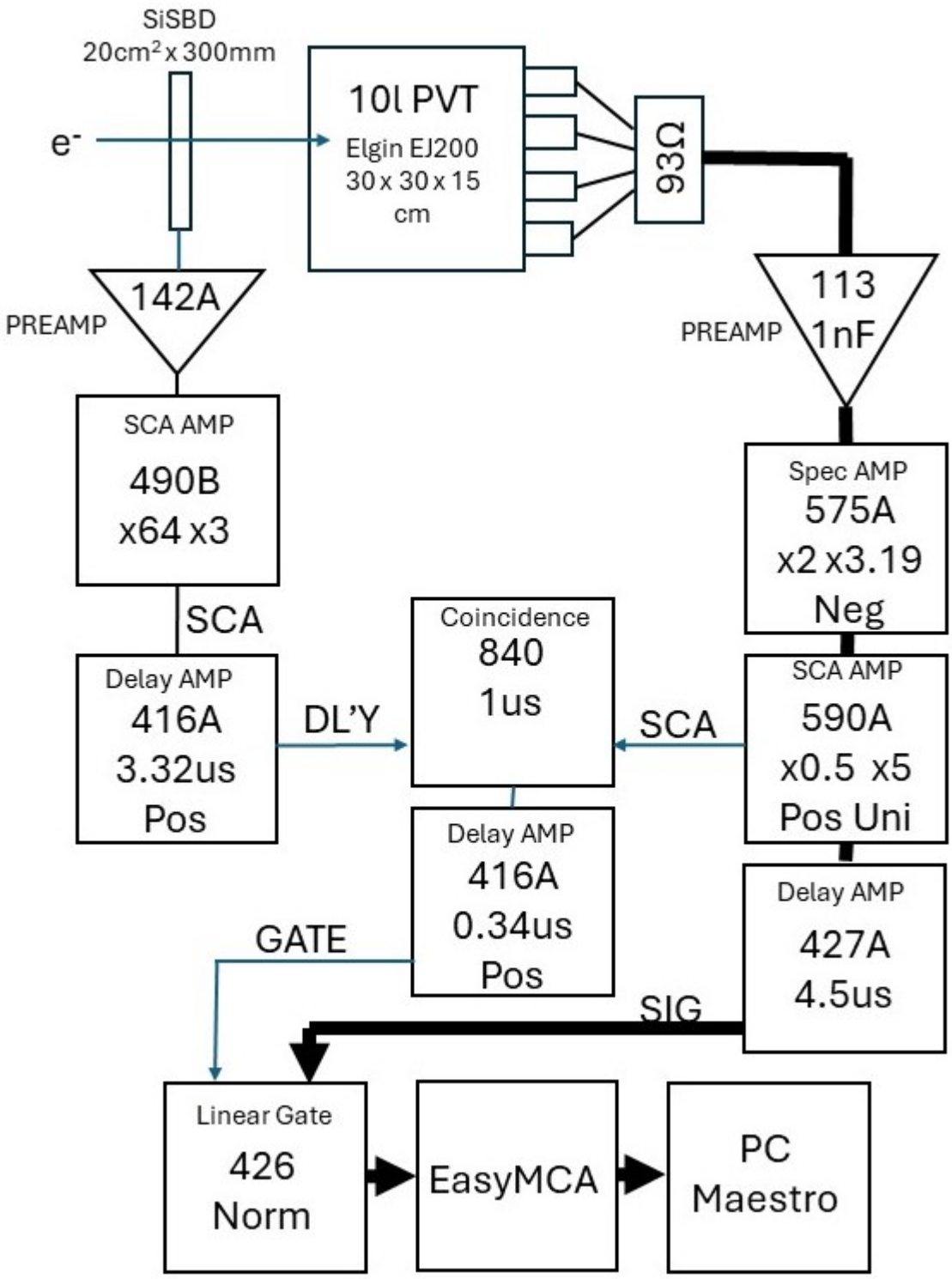

Figure 2.2 Schematic of the electronic signal processing from the detection apparatus. The setup predominantly utilizes Ortec Nuclear Instrumentation Modules, except for the Canberra-produced coincidence counter.

is fed into an Ortec 142A preamplifier [16] then into an Ortec 490B SCA amplifier [17] with a gain of 192. We take the SCA output which must be delayed in order to match the delay of the 575A-processed PVT signal. This is done using an Ortec 416A delay amplifier [18] set to delay 3.32 μs. Then, both the SCA from the silicon signal and the SCA from the PVT signal are fed into a Canberra 840 coincidence counter [19] with a resolving time of 1 μs. This is how we find which PVT signal corresponds to the silicon signal, but we still need to capture just that PVT signal.

There are again more processing delays caused by the coincidence counter, therefore the 427A delay amplifier [20] with a 4.5 μs delay was employed after the unipolar output of the 590A module. However, this delay is adjustable only in discrete quantities, so an Ortec 416A delay amplifier [18] is added after the coincidence counter. This is fine-tuned to a delay of 0.34 μs which then opens a linear gate on an Ortec 426 module [21] with the norm setting. The gate captures the coincident PVT signal and is read by an Ortec EasyMCA [22] then processed with the corresponding MCA Maestro software [23].

A simplified picture of the signal timing is depicted in Figure 2.3. It shows how the signal processing of the PVT signal delays it so the SCA signal from the silicon detector must be delayed to match it. When coincidence is found, a linear gate is triggered opening the gate. The PVT signal must be delayed to match that gate and be captured to be read and analyzed.

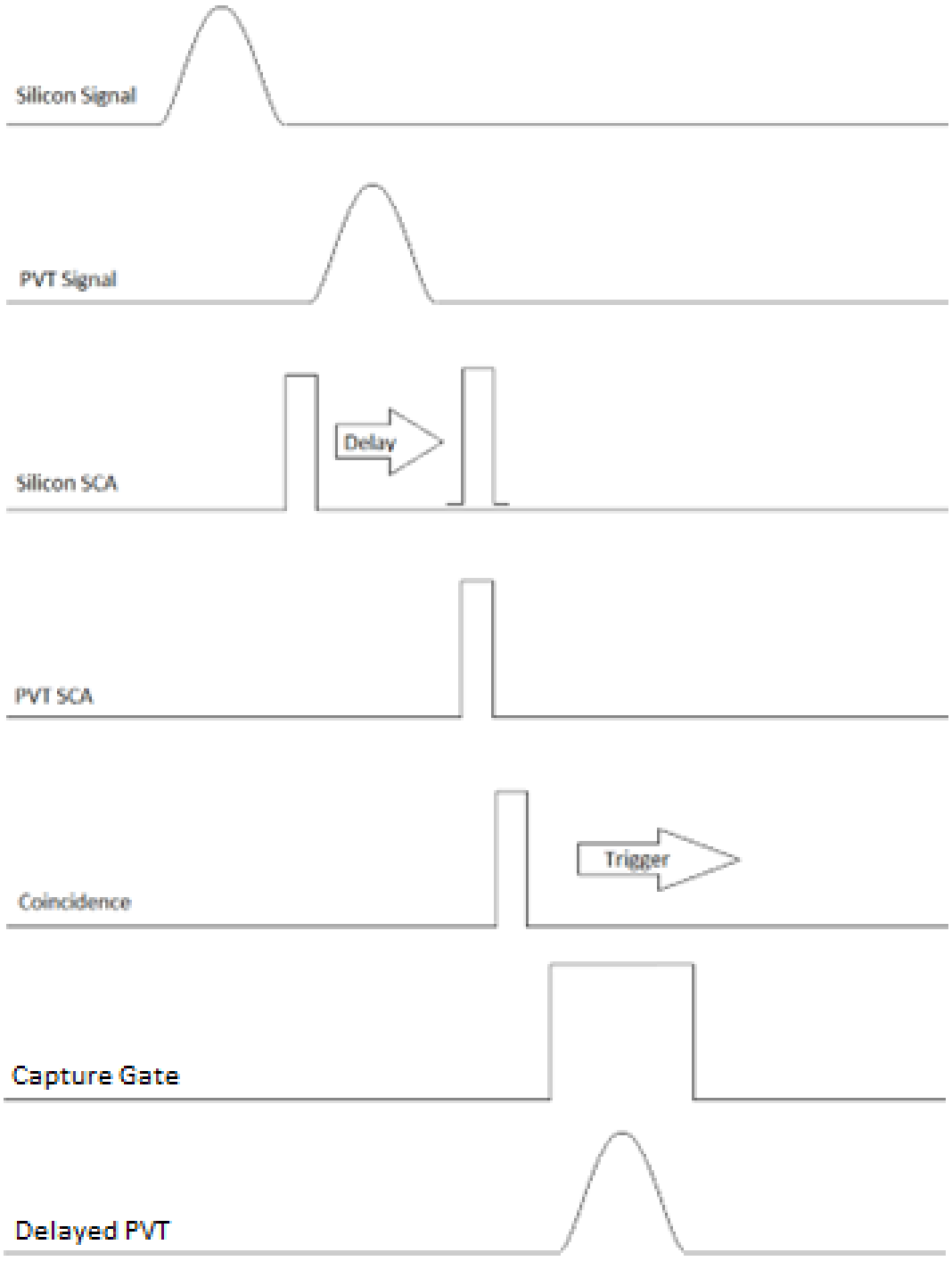

Figure 2.3 Illustration of the timing and processing of signals from both detectors, explaining how the delay in the silicon detector's signal aligns with the PVT detector's signal to ensure accurate timing and data capture.

Chapter 3

Results

To verify the spectrometer's capability to produce accurate electron spectra, we began by calibrating it using known beta-decay and conversion electron sources. We plotted the results as histograms where the x-axis represents the energy channels ranging from 0 to 255, and the y-axis indicates the count of particles detected in each channel. The known decay energies of the beta sources were crucial for assigning energy values to the channels, thus defining the energy scale for the experiment. By doing this, we could align the spectrometer's gain to capture the full energy range of interest, specifically up to 23.5 MeV, and to measure electron energies reliably in subsequent experiments.

During the calibration runs, which lasted 3000 seconds each, we accounted for the detector's energy absorption—120 keV at these energies—by shifting the calibration results by this amount. The beta-decay sources were all placed inside the target chamber at a distance of 2 inches from the detector. They were all pointing directly at the detector and were on center. The sources used were strontium-90, cesium-137, and europium-154, with radiation levels adjusted according to initial activity and date of origin at 0.98 μC, 1.04 μC, and 3.7 μC respectively.

With the strontium-90 source, the observed end-point energy of 2.28 MeV appeared at channel 115 as seen in Figure 3.1. It is important to clarify that the strontium decays into yttrium-90 which then decays further by beta-emission. The 2.28 MeV electrons are actually coming from the yttrium,

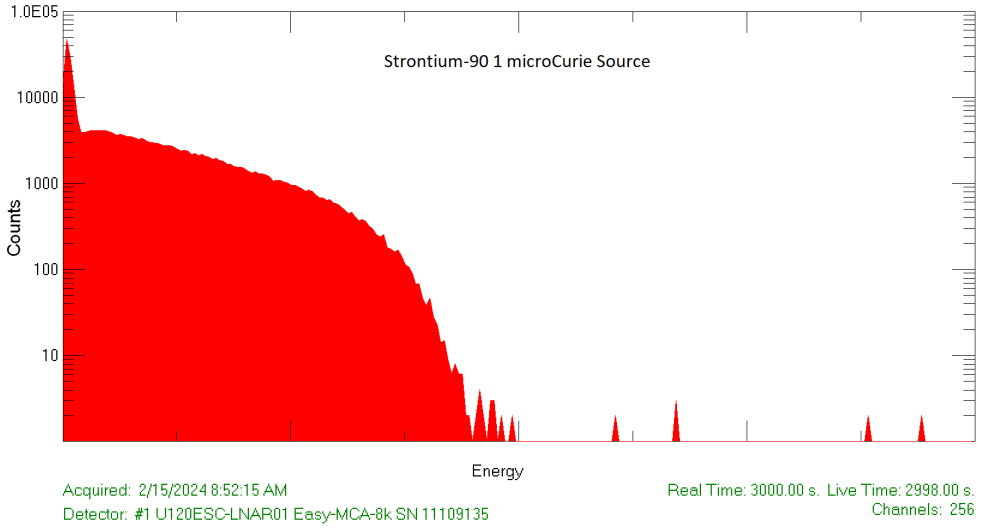

Figure 3.1 Beta decay histogram for strontium-90, showing the end-point energy at 2.28 MeV.

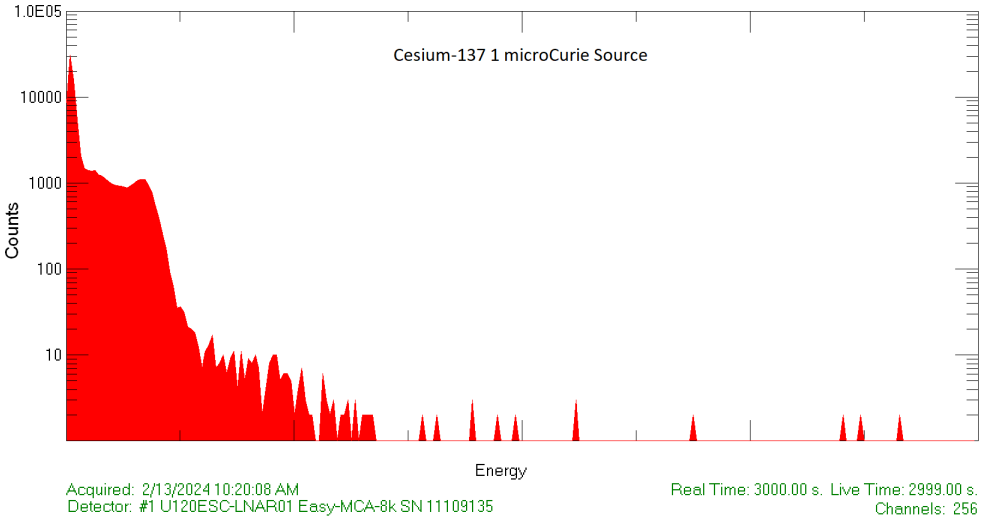

Figure 3.2 Beta decay histogram for cesium-137, with a peak energy at 0.512 MeV.

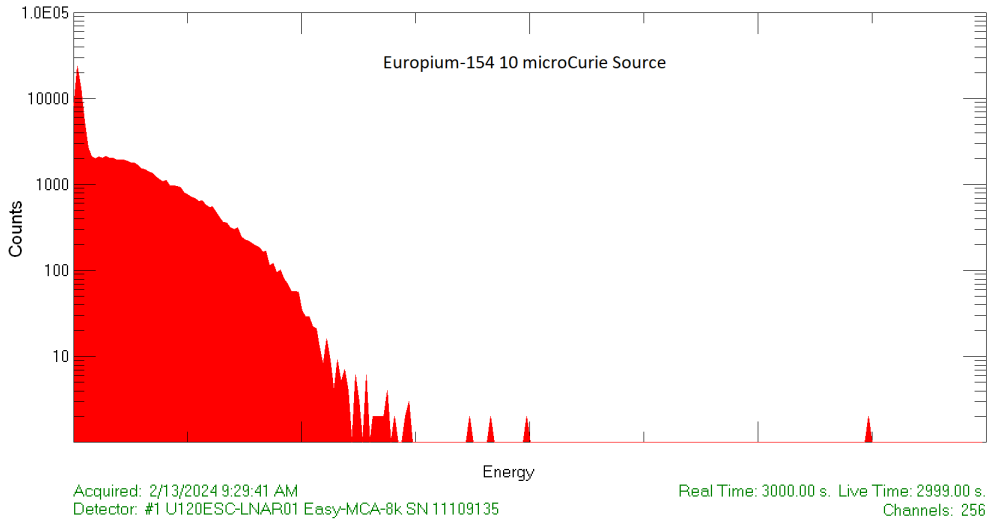

Figure 3.3 Beta decay histogram for europium-154, indicating an end-point energy of 1.9 MeV.

but the half-life is only 64 hours which is much shorter than the 28.8 year half-life of the strontium. Therefore, the rate of emission is practically the same. Thus, when I refer to the strontium-90 source, I also include the yttrium-90 with it. To detect electrons up to 23.5 MeV, the gain of the amplifiers was adjusted so that this maximum energy would coincide with channel 255. This required reducing the gain by a factor of 0.1049, setting the 2.28 MeV end-point at channel 26.

Following the same gain settings, the peak for cesium-137 at channel 22 as seen in Figure 3.2 gets mapped to channel 2 and the end-point energy observed for the europium-154 as seen in Figure 3.3 gets mapped from channel 78 to channel 8.

The background noise was also quantified to assess its impact on data quality. As Figure 3.4 demonstrates, the noise level was orders of magnitude lower compared to the beta-decay events, confirming the spectrometer's calibration and sensitivity.

A notable feature in the data was the noise following the end-point energy, attributed to double-counts. These occur when two beta-decay events are detected simultaneously, leading to an

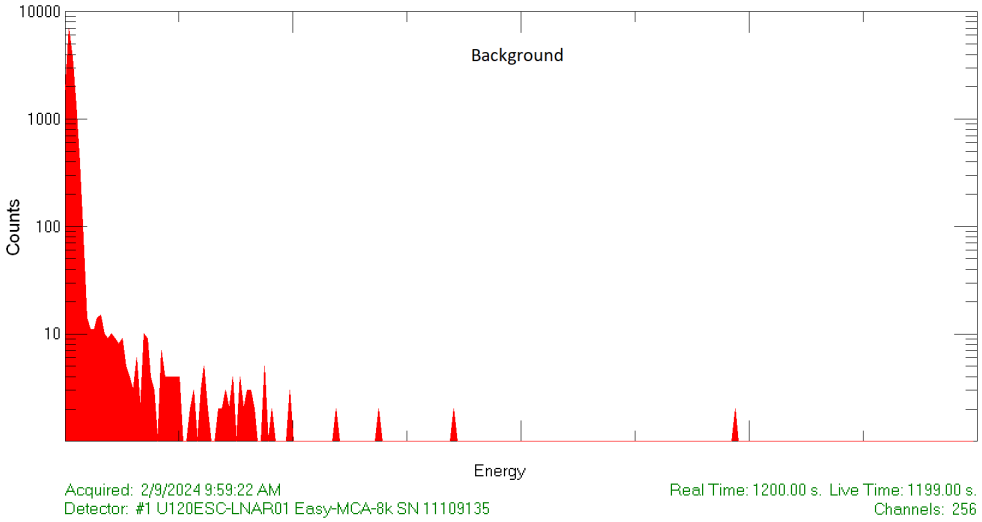

Figure 3.4 Histogram of background radiation, showing significantly lower counts than those from beta decay sources.

overestimation of energy. Understanding these double-count events is vital for ensuring precise energy measurements for future single fission occurrences.

Chapter 4

Discussion

The successful development and meticulous calibration of the high-energy electron spectrometer have been fundamental to our exploration into whether electrons can play a catalytic role in nuclear fusion reactions. Employing a dual-detector setup allowed us to precisely differentiate electrons from other particles, centering our investigative efforts on electrons that might be pivotal in fusion processes.

We calibrated the spectrometer using beta-decay and conversion electron sources. These sources were instrumental in establishing a dependable energy scale, essential for measuring the energies of electrons that are emitted from fusion events. This calibration process is critical as it mirrors the dynamics observed with conversion electrons in fission, providing a solid benchmark for our experimental setup.

Our experimental focus has been on analyzing proton-deuterium (p+d) and deuterium-deuterium (d+d) reactions. Typically, one expects to observe gamma rays as indicators of kinetic energy distribution in these reactions. However, our refined approach was to look for electrons at specific energies associated with these reactions—5.6 MeV in p+d and 23.5 MeV in d+d. Identifying electrons at these energies would suggest they have a role in facilitating these fusion reactions, akin to the role played by conversion electrons in decay processes.

The potential implications of such a discovery are profound. Confirming that electrons can catalyze fusion would help explain the significant discrepancies we currently see between the predicted and actual fusion rates observed in stellar environments. This would not only answer a crucial question in nuclear astrophysics but could also open new paths for research into lowering the barrier to fusion.

This exploration into electron-catalyzed fusion is paving the way for broader studies into lepton interactions and their potential roles in nuclear processes. The methodologies we've developed and the insights we've gained set the stage for future experiments that could vary in everything from the composition of the target to the configuration of the detectors and the range of energies explored. The discovery of electrons facilitating fusion would deepen our understanding of fundamental nuclear phenomena.

To conclude, our journey into the realm of nuclear fusion is just beginning. The findings we've discussed here represent only a fraction of the vast possibilities that await discovery. As we continue to refine our instruments and our hypotheses, we are progressively uncovering the complex interplay of particles and forces that drive the fusion processes powering the stars.

Appendix A

Testing the Energy-Dispersive X-Ray Spectrometer (EDXS)

The EDXS is an energy-dispersive X-ray spectrometer EDAX model CM200 with an active area of 30 mm^2 (see Figure A.1). The crystal is cooled with liquid nitrogen and kept under vacuum with a beryllium window. X-ray spectroscopy is an excellent tool used to characterize the elements of materials. Electrons supplied by the electron gun in Figure 2.1 will ionize the atoms in the target which will produce radiation upon relaxation. The radiation produced is a characteristic spectrum that is dependent on which elements are in the target. The EDXS collects and plots this spectrum which can show us which elements are in the target and in what ratios.

Figure A.2 shows a plot of the X-ray spectrum of an iron-55 decay source made by EDXS. Iron-55 is a common source used to calibrate X-ray spectrometers because of its two distinct peaks at 5.89 keV and 6.49 keV. The figure shows those two peaks and shows a FWHM of 190 ev.

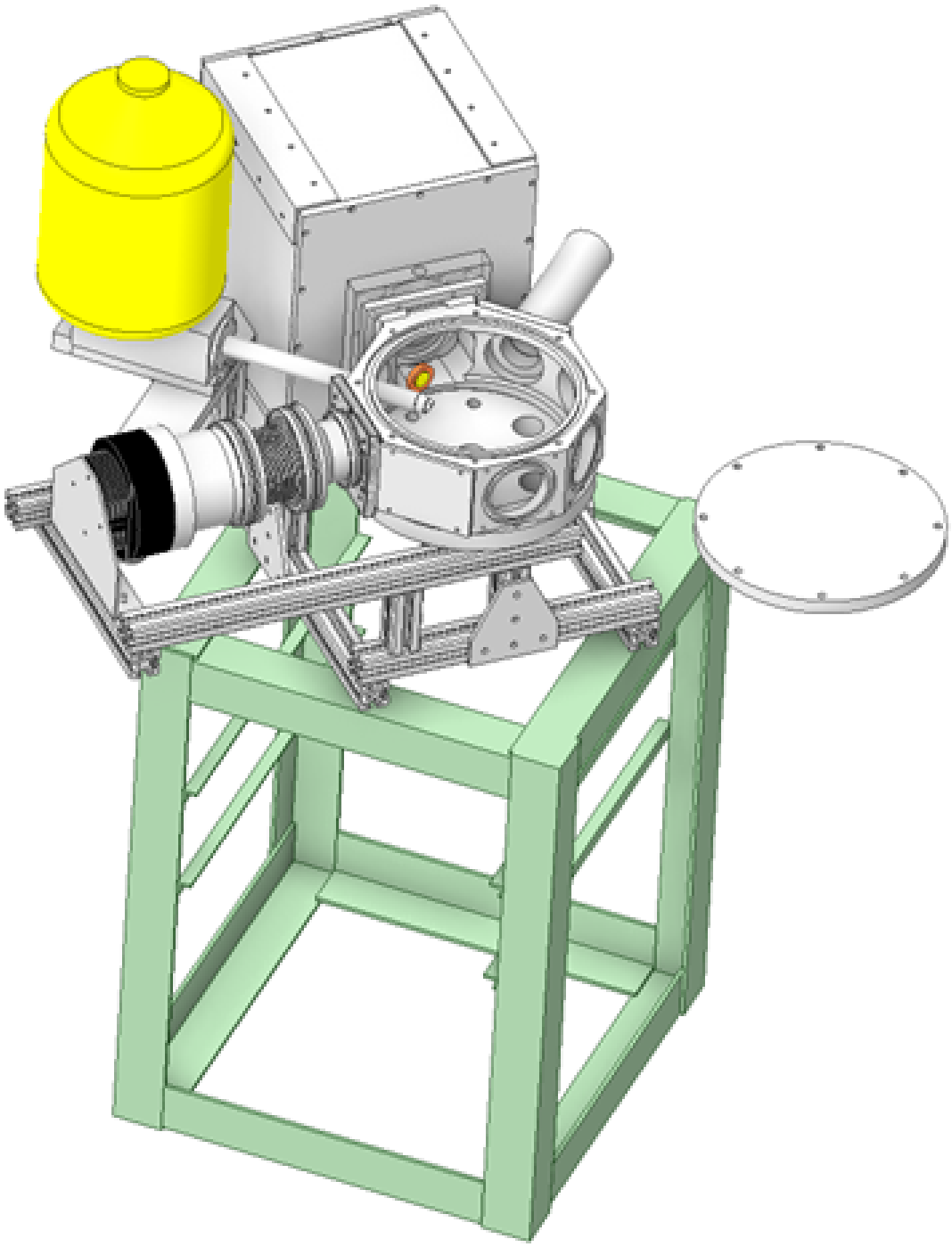

Figure A.1 This drawing depicts the target chamber with the turbo pump, high-energy electron spectrometer, EDAX, and ΔE-E detector. EDAX is highlighted in yellow and ΔE-E is highlighted in orange. The large cube is the electron spectrometer for reference.

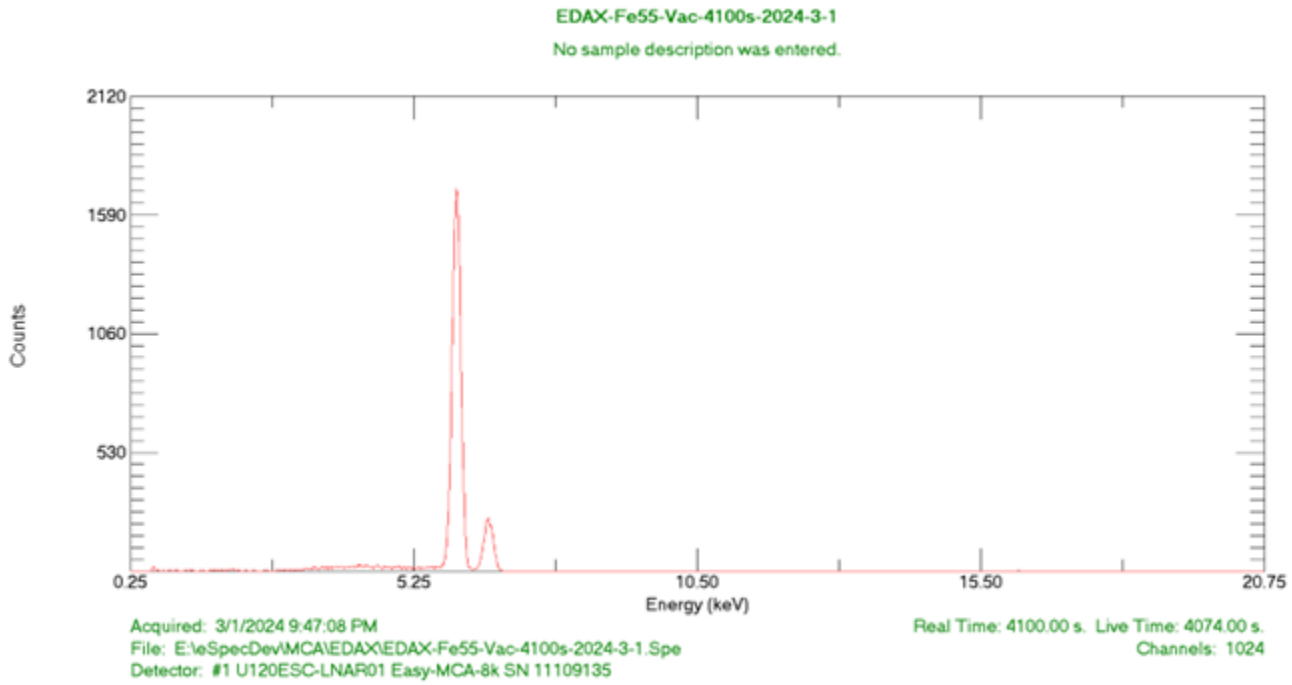

Figure A.2 This plots the X-ray spectrum of iron-55 using the energy-dispersive x-ray spectrometer (EDAX). FWHM is 190 eV.

Appendix B

Development and Testing of an ΔE-E Charged-Particle Spectrometer

The charged-particle spectrometer shares fundamental design principles with our electron spectrometer but is specifically engineered to detect a variety of heavier charged particles, such as protons, deuterons, tritons, helions, and alphas. These particles, being substantially more massive than electrons, require detectors that are less thick to effectively halt them.

The designation ΔE-E of the spectrometer reflects the method of data representation. Energy that is partially deposited by a particle in the initial, thinner detector is plotted on the y-axis, while the energy fully absorbed by the thicker stop detector is plotted on the x-axis, creating a scatter plot. This setup effectively functions as a two-dimensional multi-channel analyzer (2D MCA). Simulations, notably those conducted by Joe Hall [24] (see Figure B.2), demonstrate that distinct particle types will appear as groupings at separate locations on the scatter plot, allowing us to categorize and quantify the particle types based on their placement.

Both the initial and stop detectors used in the spectrometer are surface-barrier charged-particle detectors from Ortec. The front detector, with an area of 300 mm² and a thickness of 25 microns,

captures initial particle interactions, while the stop detector, also 300 mm² in area but 500 microns thick, ensures complete energy absorption. To mitigate noise and enhance the clarity of measurements, the detectors are encased in a cooling line filled with nitrogen gas, maintained at -38 degrees celsius.

In my experiments using an americium-241 alpha-decay source (see Figure B.1), some setups included an aluminum foil barrier of 0.18 mg/cm² to assess its impact on alpha particle energy. Interestingly, the inclusion of the foil not only reduced the energy of the alpha particles but also altered their detectable characteristics, providing insights into particle interaction with barrier materials.

For the purpose of analyzing the collected data, MATLAB software was utilized to process the digitized signals from the CAEN digitizer. The software generates histograms for both the front and stop detectors, as well as a scatter plot that displays the 2D MCA data (see Figure B.3). Additionally, I developed a menu-driven interface that allows for the examination of each event in detail, enhancing our understanding of the interaction dynamics captured by the ΔE-E detector. The code is included below.

```
% Cs137_25Mar21.m  is used to test the recently received PD2000 window
 Si detector
% Data collected using byuCaenCorder: Ch0:SiWindow, Ch1:PVT/PMT
%
clear all; close all; clc
dirs = uigetdir('','Click on directory so file names show');
files = cellstr(uigetfile([dirs,'\*.*'],'High light all files of
 interest', 'MultiSelect', 'on'));
ii=0;
for fCntr = 1 : length(files)  %get the number of data files
  fileName = [dirs, '/', char(files(fCntr))];  %create an array of
 data file names
  fid = fopen(fileName,'r');

  fseek(fid,0,'eof');
  fileLength = ftell(fid);
  fseek(fid,0,'bof');

  while ftell(fid) < fileLength - 1
    %fprintf('%d\n',ii);
    ii = ii+1;
    event(ii) = fEventRead(fid);

  end

end
  fclose('all');
%
%  event(:).ch(:,2) =-2047;
```

```
Makes a histogram of the peaks

figure
peaks = zeros(1,ii-1);
for j = 1: ii-1
  %peak(j) = (128 * max(event(j).ch(:,1))) +
 max(event(j).ch(1900:2950,2));
  %peak = max(event(j).ch(1900:2950,2));
  peak1 = max(event(j).ch(:,1));
  peak2 = max(event(j).ch(:,2));
  peaks2(:,j) = peak2;
  peaks1(:,j) = peak1;

end

  histogram(peaks1,500)
```

```
  figure
  histogram(peaks2,500)
 % set(gca,'yscale','log')
 % set(gca,'xscale','log')

%   Analyze a specific peak
gatedPeaks = zeros(ii-1,2048);
Epeaklist = zeros(1,ii-1);
Deltapeaklist = zeros(1,ii-1);
peakindices = zeros(1,438);
l = 1;
for i = 1:(ii - 1)
    Epeak = max(event(i).ch(:,2));
    Deltapeak = max(event(i).ch(:,1));
    if Epeak > 20
        Epeaklist(i) = Epeak;
        Deltapeaklist(i) = Deltapeak;
        gatedPeaks(i,:) = event(i).ch(:,1);
        peakindices(l) = i;
        l = l+1;
    end
end

% DeltaE-E plot
figure
plot(Epeaklist,Deltapeaklist,'r.')

% Case structure determines the next action to take based on user
 input
% type 'n' to show the next plot
% type 'p' to show the previous plot
% type 'number' then type the number of the plot you wish to visualize
% type 'q' to quit
% any other value will ask user to input valid value

% flag = true; m = 1;
% figure
% plot(gatedPeaks(peakindices(m),:))
% title(peakindices(m))
% while flag
%     choice = input('Enter in the first letter of the next action to
 take: ','s');
%     switch true
%         case (strcmpi(choice,'n')==1)
%             m = m+1;
%             if peakindices(m) == 0 || m <= 0
%                 fprintf('There are no more plots\n')
%             else
%                 plot(gatedPeaks(peakindices(m),:))
%                 title(peakindices(m))
%             end
%         case (strcmpi(choice,'p')==1)
%             m = m-1;
%             if m <= 0 || peakindices(m) == 0
```

```
%                 fprintf('There are no more plots\n')
%             else
%                 plot(gatedPeaks(peakindices(m),:))
%                 title(peakindices(m))
%             end
%         case (strcmpi(choice,'number')==1)
%             m = input('Enter the plot number you wish to see: ');
%             if m <= 0 || peakindices(m) == 0
%                 fprintf('This plot does not exist\n')
%             else
%                 plot(gatedPeaks(peakindices(m),:))
%                 title(peakindices(m))
%             end
%         case (strcmpi(choice,'q')==1)
%             flag = 0;
%         otherwise
%             fprintf('Please enter one of the options \n');
%     end
% end
```

Published with MATLAB® R2020a

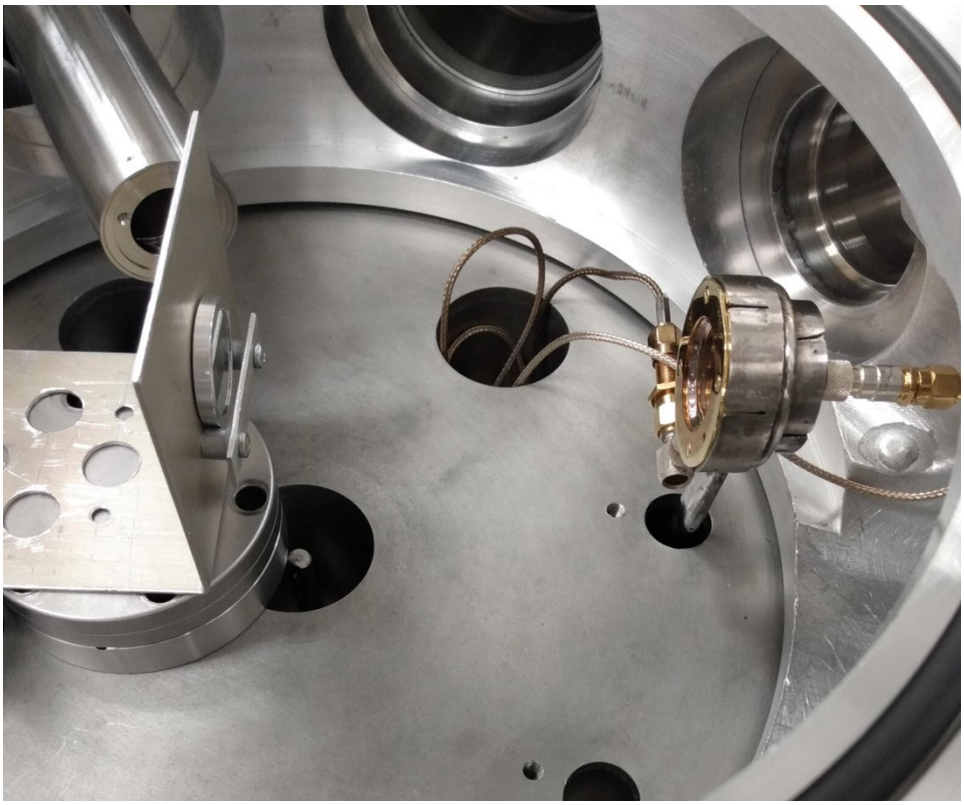

Figure B.1 Picture showing the setup of the ΔE-E detector inside the target chamber. The detector is on the right, protruding from the bottom of the chamber and the test source americium-241 is on the left.

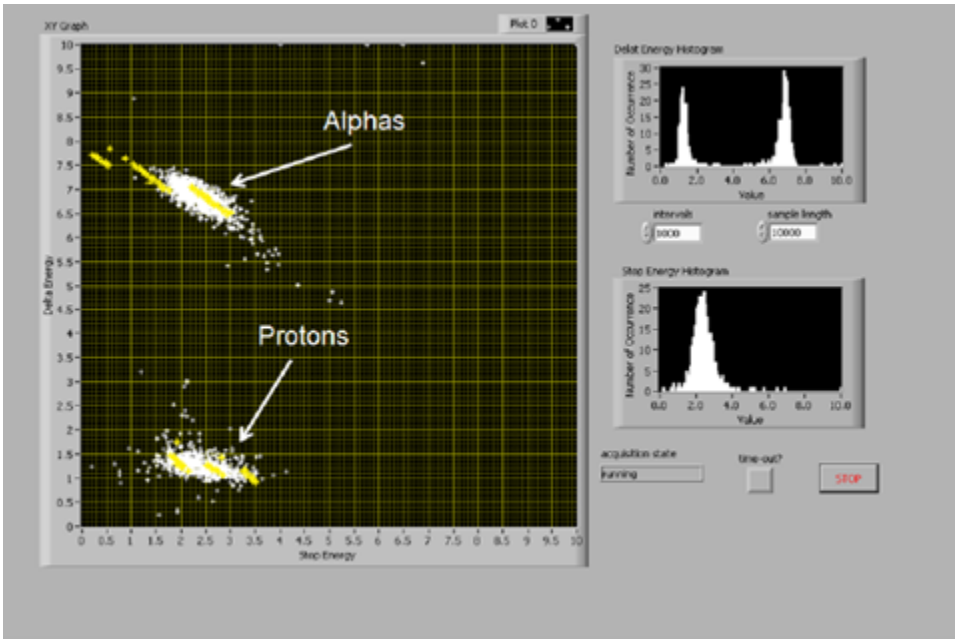

Figure B.2 Monte Carlo simulation shows the potential of the ΔE-E detector to differentiate alphas and protons. [24]

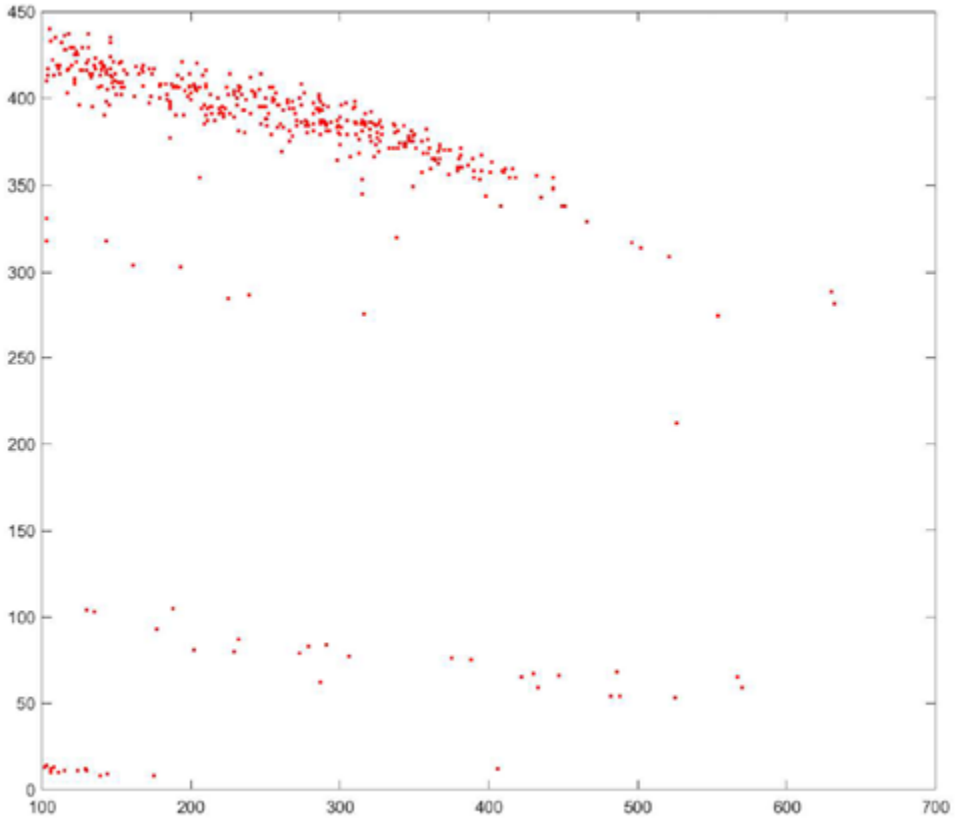

Figure B.3 Graph of the ΔE-E detector with an americium-241 source. The top grouping is unshielded and the bottom grouping is shielded by an aluminum foil of 0.18 mg/cm^2 placed in front of the detector. Note that the data collection time was significantly longer for the top grouping leading to more data points.

Bibliography

[1] J. Cruz, H. Luís, M. Fonseca, and A. P. Jesus, "Electron screening effects in nuclear reactions: still an unsolved problem," Journal of Physics: Conference Series **337,** 012062 (2012).

[2] J. Rafelski and S. E. Jones, "Cold nuclear fusion," Scientific American **257,** 84–89 (1987).

[3] S. E. Jones *et al.*, "Observation of unexpected density effects in muon-catalyzed d-t fusion," Phys. Rev. Lett. **56,** 588–591 (1986).

[4] M. Lipoglavšek, S. Markelj, M. Mihovilovič, T. Petrovič, S. Štajner, M. Vencelj, and J. Vesić, "Observation of electron emission in the nuclear reaction between protons and deuterons," Physics Letters B **773,** 553–556 (2017).

[5] H. J. Assenbaum, K. Langanke, and C. Rolfs, "Effects of electron screening on low-energy fusion cross sections," Z. Physik A - Atomic Nuclei **327,** 461–468 (1987).

[6] K. Czerski, R. Dubey, M. Kaczmarski, A. Kowalska, N. Targosz-Ślęczka, G. Das Haridas, and M. Valat, "Indications of electron emission from the deuteron-deuteron threshold resonance," Physical Review C 109 (2024).

[7] F. Raiola *et al.*, "Enhanced Electron Screening in D(D,p)t for Deuterated Metals," The European Physical Journal A **19,** 283–287 (2004).

[8] C. Rolfs, "Electron screening in metallic environments: a plasma of the poor man.," **77,** 907 (2006).

[9] A. Raymond, "Stand-alone high resolution neutron spectrometer,", 2016.

[10] *Model 04-303 Differential Ion Gun Instruction Manual*, Perkin Elmer, 2006.

[11] Ortec, *silicon charged particle radiation detectors instruction manual*, Ortec.

[12] *Model 266 Photomultiplier Base Operating and Service Manual*, Advanced Measurement Technology, Inc. a/k/a ORTEC, AMETEK Inc., 2002.

[13] *Model 113 Scintillation Preamplifier Operating and Service Manual*, Advanced Measurement Technology, Inc. a/k/a ORTEC, AMETEK Inc., 2002.

[14] *Model 575A Amplifier Operating and Service Manual*, Advanced Measurement Technology, Inc. a/k/a ORTEC, AMETEK Inc., 2002.

[15] *Model 590A Amplifier and Single-Channel Analyzer Operating and Service Manual*, Advanced Measurement Technology, Inc. a/k/a ORTEC, AMETEK Inc., 2002.

[16] *Models 142A, 142B, and 142C Preamplifiers Operating and Service Manual*, Advanced Measurement Technology, Inc. a/k/a ORTEC, AMETEK Inc., 2002.

[17] *ORTEC 490B Amplifier and Single Channel Analyzer Operating and Service Manual*, Ortec Incorporated, 100 Midland Rd., Oak Ridge, Tenn., 1970.

[18] *Model 416A Gate and Delay Generator Operating and Service Manual*, Advanced Measurement Technology, Inc. a/k/a ORTEC, AMETEK Inc., 2002.

[19] *Coincidence Analyzer 840*.

[20] *Model 427A Delay Amplifier Operating and Service Manual*, Advanced Measurement Technology, Inc. a/k/a ORTEC, AMETEK Inc., 2002.

[21] *Model 426 Linear Gate Operating and Service Manual*, Advanced Measurement Technology, Inc. a/k/a ORTEC, AMETEK Inc., 2002.

[22] *EASY-MCA-8K EASY-MCA-2K Digital Gamma-Ray Spectrometer Hardware User's Manual*, Advanced Measurement Technology, Inc., 2009.

[23] *MAESTRO-32 MCA Emulator for Microsoft Windows 2000 Professional, XP Professional SP2, and Vista Ultimate*, Advanced Measurement Technology, Inc., 2008, software Ver 6.0.

[24] J. Hall, "Assembly of a beam target chamber for studying screening potentials in condensed matter.", 2017.

List of Figures

Index